Radiation Properties of Circumferential Slots on a Coaxial Cable

Jean-Fu Kiang, *Member, IEEE*

***Abstract*—Both the Galerkin's and mode-matching methods are used to analyze the reflection and radiation properties of a coaxial cable with a circumferential slot on the outer conductor. The effects of higher order modes are also included. The accumulated effect of multiple slots on the reflected signal is also studied by using a Monte Carlo simulation.**

***Index Terms*— Coaxial cable, Galerkin's method, mode-matching, Monte Carlo simulation, slot radiation.**

I. Introduction

SLOT ANTENNAS have been used on vehicle surfaces due to their conformability and power handling capacity. Slots in different environments having been studied are a circumferential slot on a cylindrical waveguide surface (for its admittance) [1], a slanted slot on a cylindrical surface (formed by terminating a rectangular waveguide) [2], a rectangular slot backed by a cylindrical cavity [3], a narrow longitudinal slot on a sectoral waveguide [4], and so on. Another problem related to slot radiation is the electric field distribution across the feed gap of a cylindrical dipole antenna [5]. An annular aperture can be formed by attaching a ground plane to the opening of a coaxial cable and serves as a slot antenna or a sensor [6], [7]. Segments of coaxial cables can be connected to form a coaxial collinear antenna [8]. The equivalent voltages across the slot gaps are solved first to calculate the current distribution on the outer surface.

In this paper, we study the radiation properties of slots on a coaxial cable that can be used to distribute signals in a wireless local area network. The coaxial cable can be used to transmit signals over a much longer distance than antennas. Slots on the coaxial cable can be opened to transmit signals to local users without interfering with other electronic equipments far away from them. The dominant TEM mode propagating in the cable induces higher order modes around the slots and is itself partly reflected. The reflections induced by different slots along the cable may accumulate and reduce the transmission efficiency. Hence, we will first study the reflection and radiation characteristics of a circumferential slot on the outer conductor of a coaxial cable by using both the Galerkin's and the mode-matching methods. Then, a Monte Carlo simulation will be used to analyze the accumulated effects of multiple slots on the reflected power.

Manuscript received April 28, 1996; revised September 23, 1996. This work was supported by the National Science Council under Contract NSC86-2221-E005-021.

The author is with the Department of Electrical Engineering, National Chung-Hsing University, Taichung, Taiwan, R.O.C.

Publisher Item Identifier S 0018-9480(97)00272-X.

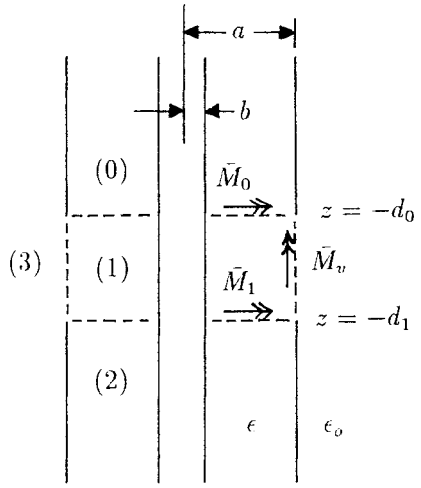

Fig. 1. Geometrical configuration of a coaxial cable with a circumferential slot.

II. Galerkin's Method

In Fig. 1, we show a circumferential slot cut on the outer conductor of a coaxial cable, and the space is divided into four regions. The radii of the inner and the outer conductor of the coaxial are b and a. Assume that a TEM mode propagates from $z = -\infty$ toward region (1) and that a reflected TEM mode and the higher-order TM modes are induced and propagate in the $-z$ direction in region (2). In region (0) above the slot, a TEM mode and the higher order TM modes are induced and propagate in the z direction.

An equivalent problem can be formed in each region. The magnetic surface current $\overline{M}_0$ generates the fields in region (0), the magnetic surface current $-\overline{M}_1$ generates the fields in region (2), the magnetic surface current $-\overline{M}_0, \overline{M}_1$, and $\overline{M}_v$ generate the fields in region (1), and the magnetic surface current $-\overline{M}_v$ generates the fields in region (3) outside of the cable.

First expand the fields in each region in terms of the eigenmodes as [9], [10]

$$E_{0\rho} = \sum_{n=0}^{\infty} S_n(\rho) e_{0n} \frac{k_{nz}}{\omega\epsilon} e^{ik_{nz}z_0}$$

$$H_{0\phi} = \sum_{n=0}^{\infty} S_n(\rho) e_{0n} e^{ik_{nz}z_0}$$

$$E_{1\rho} = -\sum_{n=0}^{\infty} S_n(\rho) \frac{k_{nz}}{i\omega\epsilon} [e_{1n}^a \sin k_{nz}z_1 + e_{1n}^b \sin k_{nz}(z_1 - h_1)]$$

$$
\begin{aligned}
H_{1\phi} &= \sum_{n=0}^{\infty} S_n(\rho)[e_{1n}^a \cos k_{nz} z_1 + e_{1n}^b \cos k_{nz}(z_1 - h_1)] \\
&\quad + e_{10}^c [J_1(k\rho)N_0(kb) - J_0(kb)N_1(k\rho)] \\
E_{1z} &= -\frac{1}{i\omega\epsilon} \sum_{n=1}^{\infty} \frac{1}{\rho}\frac{\partial}{\partial\rho}\rho S_n(\rho)[e_{1n}^a \cos k_{nz} z_1 \\
&\quad + e_{1n}^b \cos k_{nz}(z_1 - h_1)] \\
&\quad - \frac{k}{i\omega\epsilon} e_{10}^c [J_0(k\rho)N_0(kb) - J_0(kb)N_0(k\rho)] \\
E_{2\rho} &= -\sum_{n=0}^{\infty} S_n(\rho) e_{2n} \frac{k_{nz}}{\omega\epsilon} e^{-ik_{nz}z_2} + S_0(\rho)\frac{k_{0z}}{\omega\epsilon} e^{ik_{0z}z_2} \\
H_{2\phi} &= \sum_{n=0}^{\infty} S_n(\rho) e_{2n} e^{-ik_{nz}z_2} + S_0(\rho) e^{ik_{0z}z_2} \\
E_{3z} &= \int_{-\infty}^{\infty} dk_z e(k_z) e^{ik_z z_1} H_0^{(1)}(k_\rho \rho) \\
H_{3\phi} &= -\int_{-\infty}^{\infty} dk_z e(k_z) e^{ik_z z_1} \frac{i\omega\epsilon_o}{k_\rho} H_1^{(1)}(k_\rho\rho)
\end{aligned} \tag{1}
$$

where

$$
k = \omega\sqrt{\epsilon\mu_o}, \quad k_\rho = \sqrt{\omega^2\mu_o\epsilon_o - k_z^2}, \quad z_0 = z + d_0
$$
$$
z_1 = z + d_1, \quad z_2 = z + d_1, \quad \text{and} \quad h_1 = d_1 - d_0
$$

is the width of the slot. $S_n(\rho)$'s with $n \geq 1$ are the ρ-dependence of the TM_n mode, and $S_0(\rho)$ is that of the TEM mode. Explicitly

$$
S_n(\rho) = C_n^{-1}[J_1(\xi_n\rho/a)N_0(\xi_n) - J_0(\xi_n)N_1(\xi_n\rho/a)]
$$

with $n \geq 1$ and

$$
J_0(\xi_n b/a)N_0(\xi_n) - J_0(\xi_n)N_0(\xi_n b/a) = 0,
$$
$$
S_0(\rho) = [\sqrt{\log(a/b)}\rho]^{-1}.
$$

The normalization constants $\{C_n\}$ are chosen such that $\int_b^a S_m(\rho)S_n(\rho)\rho\, d\rho = \delta_{mn}$, k_{nz} is the propagation constant in the z direction of the TM_n mode and is related to the eigenvalue ξ_n by $k_{nz}^2 + (\xi_n/a)^2 = k^2$.

Due to the configuration symmetry, the magnetic surface currents $\overline{M}_0$ and $\overline{M}_1$ have only ϕ-components and can be expanded in terms of $S_n(\rho)$'s as

$$
M_i(\rho) = \sum_{n=0}^{\infty} M_{in} S_n(\rho), \qquad i = 0, 1. \tag{2}
$$

Also, the magnetic surface current $\overline{M}_v$ has only a ϕ-component. Assuming that the slot width is much smaller than one wavelength, M_v can be approximated as a constant $M_{v\phi}$.

Next, apply the following boundary conditions:

$$
\begin{aligned}
\overline{M}_0 &= \overline{E}_0 \times \hat{z} \text{ at } z = -d_0 + \varepsilon \\
-\overline{M}_0 &= \overline{E}_1 \times (-\hat{z}) \text{ at } z = -d_0 - \varepsilon \\
\overline{M}_1 &= \overline{E}_1 \times \hat{z} \text{ at } z = -d_1 + \varepsilon \\
-\overline{M}_1 &= \overline{E}_2 \times (-\hat{z}) \text{ at } z = -d_1 - \varepsilon \\
\overline{M}_v &= \overline{E}_1 \times (-\hat{\rho}) \text{ at } \rho = a - \varepsilon \\
-\overline{M}_v &= \overline{E}_3 \times \hat{\rho} \text{ at } \rho = a + \varepsilon
\end{aligned} \tag{3}
$$

where ε is an infinitesimal positive number. Thus, we have

$$
\begin{aligned}
e_{0n} &= -\frac{\omega\epsilon}{k_{nz}} M_{0n} \\
e_{1n}^a &= \frac{i\omega\epsilon}{k_{nz}} \frac{1}{\sin k_{nz} h_1} M_{0n} \\
e_{1n}^b &= -\frac{i\omega\epsilon}{k_{nz}} \frac{1}{\sin k_{nz} h_1} M_{1n} \\
e_{2n} &= \delta_{n0} + \frac{\omega\epsilon}{k_{nz}} M_{1n} \\
e_{10}^c &= \frac{i\omega\epsilon}{k}[J_0(ka)N_0(kb) - J_0(kb)N_0(ka)]^{-1} M_{v\phi} \\
e(k_z) &= -\frac{M_v(k_z)}{H_0^{(1)}(k_\rho a)}
\end{aligned} \tag{4}
$$

where

$$
M_v(k_z) = \frac{M_{v\phi}}{2\pi} \int_0^{h_1} e^{-ik_z z_1}\, dz_1.
$$

Substitute the relations in (4) into the field expressions in (1), then apply the following boundary conditions to obtain three continuity equations:

$$
H_{0\phi} = H_{1\phi} \text{ at } z = -d_0 \tag{5}
$$
$$
H_{1\phi} = H_{2\phi} \text{ at } z = -d_1 \tag{6}
$$
$$
H_{1\phi} = H_{3\phi} \text{ at } \rho = a, \qquad 0 \leq z_1 \leq h_1. \tag{7}
$$

To apply the Galerkin method, first choose a set of basis functions to represent the magnetic surface current as

$$
M_i(\rho) = \sum_{p=0}^{N-1} \alpha_{ip} f_p(\rho), \qquad i = 0, 1 \tag{8}
$$

where

$$
f_p(\rho) = \begin{cases} (a-b)^{-1}\cos[p\pi(\rho - b)/(a-b)], & b \leq \rho \leq a \\ 0, & \text{elsewhere.} \end{cases} \tag{9}
$$

Next, choose the same set of basis functions as the weighting functions. Then, multiply (5) and (6) by $\rho f_q(\rho)$ and integrate over the interval $b \leq \rho \leq a$ to have

$$
\begin{aligned}
&\sum_{p=0}^{N-1} \alpha_{0p} \sum_{n=0}^{\infty} f_{qn} \frac{\omega\epsilon}{k_{nz}}(1 + i\cot k_{nz} h_1) f_{pn} \\
&\quad - \sum_{p=0}^{N-1} \alpha_{1p} \sum_{n=0}^{\infty} f_{qn} \frac{i\omega\epsilon}{k_{nz}}(\csc k_{nz} h_1) f_{pn} \\
&\quad + M_{v\phi}\frac{i\omega\epsilon}{k}\int_b^a d\rho\, \rho f_q(\rho) R_0(\rho) = 0, \\
&\qquad 0 \leq q \leq N-1
\end{aligned} \tag{10}
$$

$$
\begin{aligned}
&\sum_{p=0}^{N-1} \alpha_{0p} \sum_{n=0}^{\infty} f_{qn} \frac{i\omega\epsilon}{k_{nz}}(\csc k_{nz} h_1) f_{pn} \\
&\quad - \sum_{p=0}^{N-1} \alpha_{1p} \sum_{n=0}^{\infty} f_{qn} \frac{\omega\epsilon}{k_{nz}}(1 + i\cot k_{nz} h_1) f_{pn} \\
&\quad + M_{v\phi}\frac{i\omega\epsilon}{k}\int_b^a d\rho\, \rho f_q(\rho) R_0(\rho) = 2f_{q0}, \\
&\qquad 0 \leq q \leq N-1
\end{aligned} \tag{11}
$$

where

$$f_{pn} = \int_b^a \rho\, d\rho\, f_p(\rho) S_n(\rho)$$
$$R_0(\rho) = \frac{J_1(k\rho)N_0(kb) - J_0(kb)N_1(k\rho)}{J_0(ka)N_0(kb) - J_0(kb)N_0(ka)}. \tag{12}$$

Finally, integrate (7) over the interval $0 \le z_1 \le h_1$ to have

$$\sum_{p=0}^{N-1} \alpha_{0p} \sum_{n=0}^{\infty} S_n(a) \frac{i\omega\epsilon}{k_{nz}^2} f_{pn} - \sum_{p=0}^{N-1} \alpha_{1p} \sum_{n=0}^{\infty} S_n(a) \frac{i\omega\epsilon}{k_{nz}^2} f_{pn} + M_{v\phi} \left[h_1 \frac{i\omega\epsilon}{k} R_0(a) - \frac{h_1^2}{2\pi} \int_{-\infty}^{\infty} dk_z\, \mathrm{sinc}^2(k_z h_1/2) \cdot \frac{i\omega\epsilon_o}{k_\rho} \frac{H_1^{(1)}(k_\rho a)}{H_0^{(1)}(k_\rho a)} \right] = 0 \tag{13}$$

where $\mathrm{sinc}(x) = \sin(x)/x$. Once the unknowns α_{0p}, α_{1p}, and $M_{v\phi}$ are solved from (10), (11), and (13), the field distributions are obtained. The coefficient e_{20} in (1) is the reflection coefficient, and e_{00} is the transmission coefficient of the incident TEM mode due to the slot.

III. Mode-Matching Method

The mode-matching method is an alternative to solve for the field distribution in all regions by matching the tangential electric and magnetic fields across the interfaces. Impose the following boundary conditions: 1) $E_{0\rho} = E_{1\rho}$ at $z = -d_0$; 2) $H_{0\phi} = H_{1\phi}$ at $z = -d_0$; 3) $E_{1\rho} = E_{2\rho}$ at $z = -d_1$; 4) $H_{1\phi} = H_{2\phi}$ at $z = -d_1$; 5) $H_{1\phi} = H_{3\phi}$ at $\rho = a$ and $0 \le z_1 \le h_1$. Then, apply the orthonormality properties of $S_n(\rho)$'s to have

$$e_{0n} = e_{1n}^a i \sin k_{nz} h_1, \qquad 0 \le n < \infty$$
$$e_{0n} = e_{1n}^a \cos k_{nz} h_1 + e_{1n}^b + \frac{i\omega\epsilon}{k} M_{v\phi} \int_b^a \rho\, d\rho\, S_n(\rho) R_0(\rho), \qquad 0 \le n < \infty$$
$$e_{1n}^b \sin k_{nz} h_1 = i(\delta_{n0} - e_{2n}), \qquad 0 \le n < \infty$$
$$e_{1n}^a + e_{1n}^b \cos k_{nz} h_1 + \frac{i\omega\epsilon}{k} M_{v\phi} \int_b^a \rho\, d\rho\, S_n(\rho) R_0(\rho) = \delta_{n0} + e_{2n}, \qquad 0 \le n < \infty$$
$$\sum_{n=0}^{\infty} S_n(a) \frac{\sin k_{nz} h_1}{k_{nz}} (e_{1n}^a + e_{1n}^b) + M_{v\phi} \left[h_1 R_0(a) \frac{i\omega\epsilon}{k} - \frac{h_1^2}{2\pi} \int_{-\infty}^{\infty} dk_z\, \mathrm{sinc}^2(k_z h_1/2) \frac{i\omega\epsilon_o}{k_\rho} \frac{H_1^{(1)}(k_\rho a)}{H_0^{(1)}(k_\rho a)} \right] = 0. \tag{14}$$

Truncate each series in (14) into N terms ($0 \le n < N$). Then, (14) contains $4N + 1$ equations. The coefficients $e_{0n}, e_{1n}^a, e_{1n}^b, e_{2n}$, and $M_{v\phi}$ are obtained by solving these equations.

IV. Radiation Fields

By using either the Galerkin's or the mode-matching method, the far field can be calculated in the same manner. From (1) and (4), the E_z component in region (3) can be expressed in terms of the magnetic surface current $M_v(k_z)$. In the far field zone, the Hankel function can be approximated by its asymptotic form. The stationary phase approximation is then applied to obtain the far field as

$$E_z \approx \frac{e^{ik_o r}}{r} 2i \frac{M_v(k_o \cos\theta)}{H_0^{(1)}(k_o a \sin\theta)} \tag{15}$$

where $k_o = \omega\sqrt{\mu_o\epsilon_o}$, the observation point is at $\rho = r\sin\theta$ and $z_1 = r\cos\theta$. The E_θ and H_ϕ components are related to E_z by $E_\theta = -E_z/\sin\theta, H_\phi = E_\theta/\sqrt{\mu_o/\epsilon_o}$.

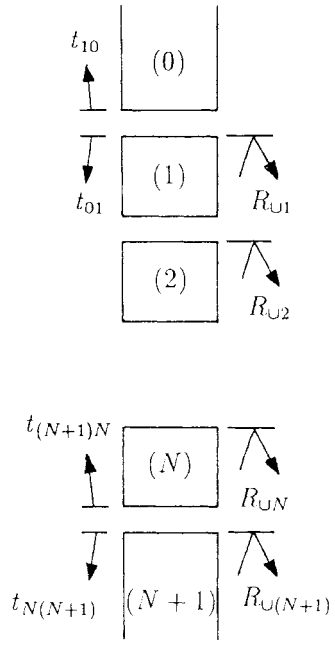

Fig. 2. Configuration to calculate the total reflection coefficients recursively.

V. Accumulated Reflection

Fig. 2 shows a coaxial cable with $N + 1$ slots. In practice, the electrical length between any two neighboring slots cannot be adjusted to within a fraction of one wavelength in precision. Thus, we may assume that the phase difference between any two neighboring slots has a uniform probability distribution in $[0, 2\pi]$.

Define the local reflection coefficient r_{ij} as the ratio of the reflected wave to the incident wave where the incident wave is propagating in coaxial segment i toward the slot between segments i and j where $j = i \pm 1$. Also define the local transmission coefficient t_{ij} as the ratio of the transmitted wave in coaxial segment j to the incident wave in coaxial segment i where $j = i \pm 1$. Both coefficients are calculated by the Galerkin's or the mode-matching method. Define the total reflection coefficient $R_{\cup l}$ at the lth slot between coaxial segments $l-1$ and l as the ratio of the TEM wave propagating in the $-\hat{z}$ direction to that propagating in the $\hat{z}$ direction at the slot.

At the first slot, $R_{\cup 1} = r_{10}$. By tracing all the reflected waves, the total reflection coefficient at the second slot can be calculated as

$$R_{\cup 2} = r_{21} + t_{21} \frac{\alpha_1^2 R_{\cup 1}}{1 - \alpha_1^2 R_{\cup 1} r_{12}} t_{12} \tag{16}$$

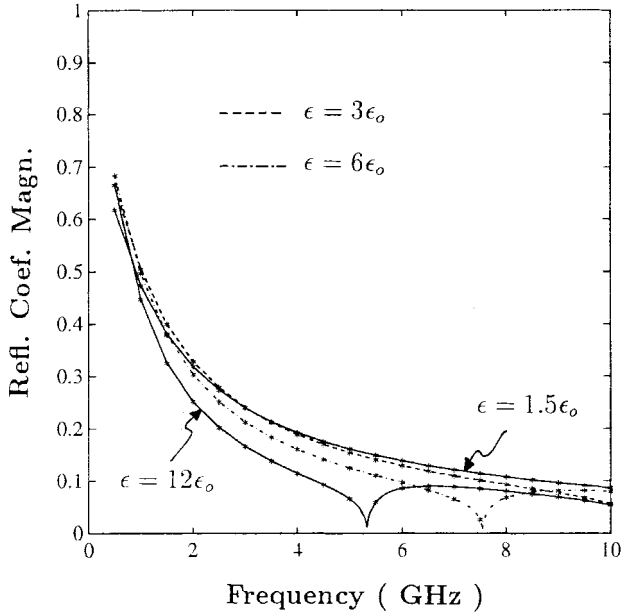

Fig. 3. Effects of the dielectric constant on the reflection coefficient of the TEM mode, $a = 1.2$ cm, $b = 0.4$ cm, $h_1 = 0.1$ cm, *: mode-matching method.

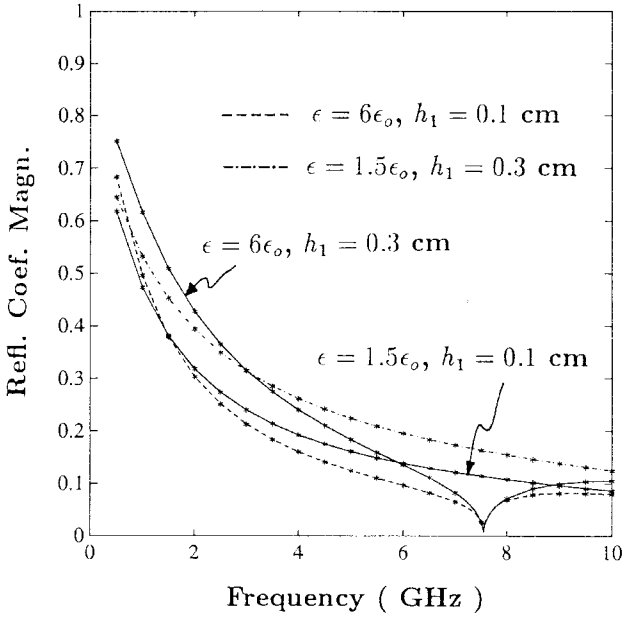

Fig. 5. Effects of the slot width on the reflection coefficient of the TEM mode. $a = 1.2$ cm, $b = 0.4$ cm, *: mode-matching method.

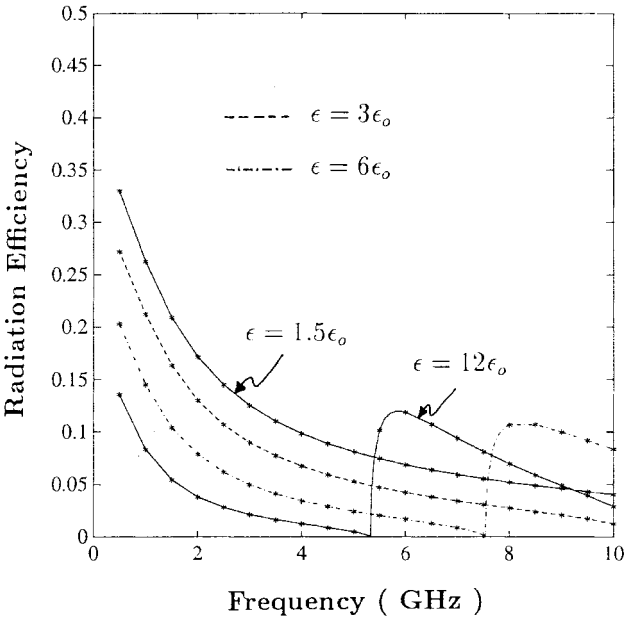

Fig. 4. Effects of the dielectric constant on the radiation efficiency of the slot. The parameters are the same as in Fig. 3.

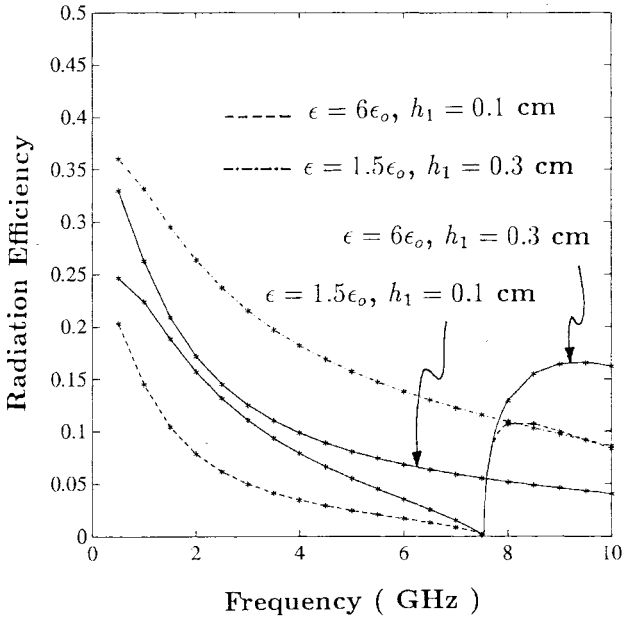

Fig. 6. Effects of the slot width on the radiation efficiency of the slot. The parameters are the same as in Fig. 5.

where $\alpha_1 = e^{ikh_1}$ is the propagation factor for the TEM wave to propagate over the segment length h_1. The ratio in (16) can be expanded as an infinite series with each term representing one possible wave trace in the first coaxial segment. This procedure can be repeated from the second to the $(N+1)$th slot as

$$R_{\cup l} = r_{l(l-1)} + t_{l(l-1)} \frac{\alpha_{l-1}^2 R_{\cup(l-1)}}{1 - \alpha_{l-1}^2 R_{\cup(l-1)} r_{(l-1)l}} t_{(l-1)l}, \quad l = 2, \cdots, N+1. \tag{17}$$

Assume that e^{ikh_l} has a uniformly distributed phase over $[0, 2\pi]$ for $l = 1, \cdots, N+1$. Then apply a Monte Carlo simulation over the phase of all the e^{ikh_l} terms in (17) to obtain a probability distribution of the reflection coefficient magnitude $|R_{\cup(N+1)}|$.

VI. Numerical Results

In all the cases to be presented, the curves are obtained by applying the Galerkin's method, and the *-marked results are obtained by using the mode-matching technique. In Fig. 3, we show the reflection coefficient magnitude of the dominant TEM mode caused by a slot of width 0.1 cm. The reflection coefficient decreases with increasing frequency. The magnitude

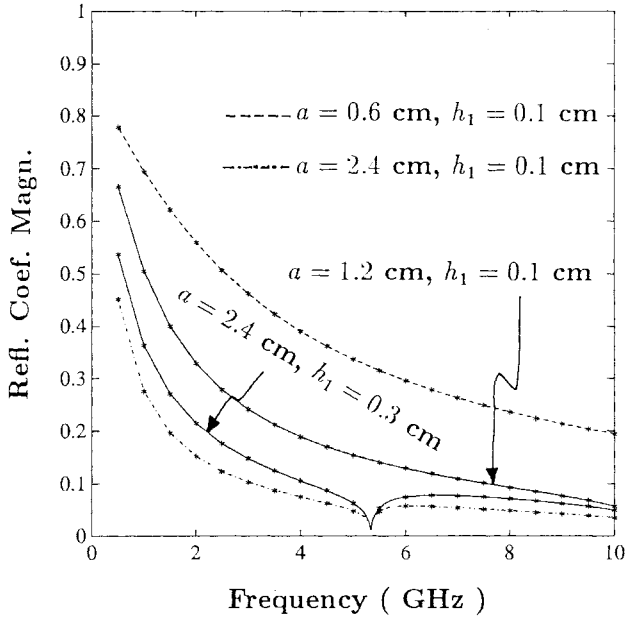

Fig. 7. Effects of the coaxial radius on the reflection coefficient of the TEM mode. $a/b = 3, \epsilon = 3\epsilon_o$ cm, *: mode-matching method.

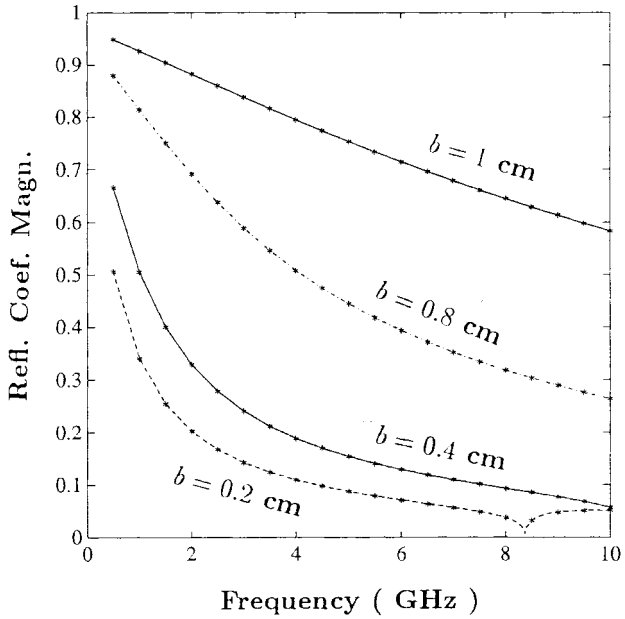

Fig. 9. Effects of the coaxial radii ratio on the reflection coefficient of the TEM mode. $a = 1.2$ cm, $h_1 = 0.1$ cm, $\epsilon = 3\epsilon_o$, *: mode-matching method.

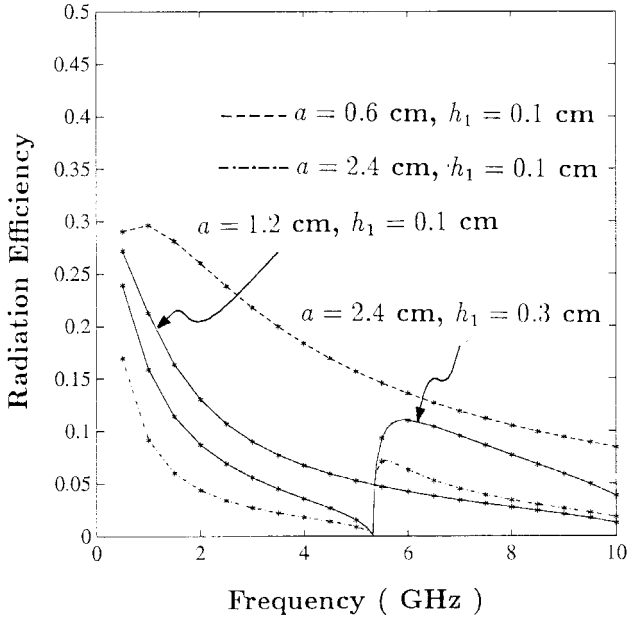

Fig. 8. Effects of the coaxial radius on the radiation efficiency of the slot. The parameters are the same as in Fig. 7.

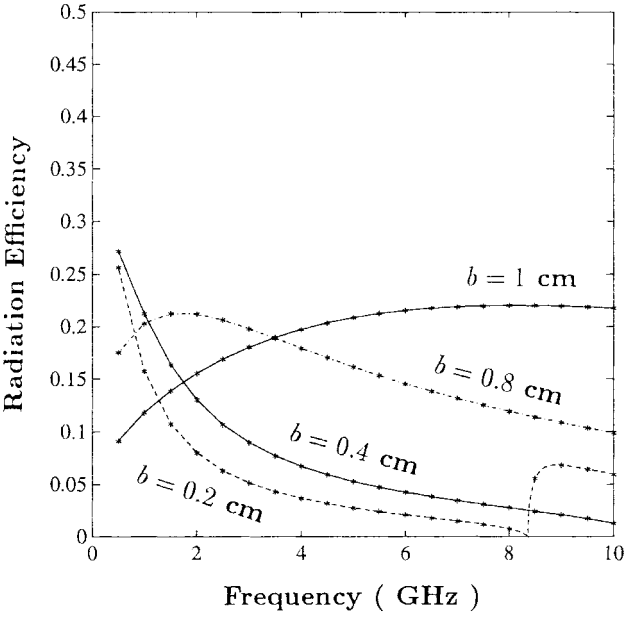

Fig. 10. Effects of the coaxial radii ratio on the radiation efficiency of the slot, the parameters are the same as in Fig. 9.

decreases when the permittivity inside the coaxial is increased from $1.5\epsilon_o$ to $3\epsilon_o$. When the permittivity is further increased to $6\epsilon_o$ and $12\epsilon_o$, the reflection coefficient has a null around the cutoff frequency of the TM_1 mode.

The radiation from the slot is observed to have a nearly omnidirectional pattern in the range of $5° < \theta < 175°$, which is a good feature for signal distribution. Define the radiation efficiency as the ratio of the radiated power to the incident power. It is equal to $1 - |R|^2 - |T|^2$ by power conservation, where R and T are the local reflection and transmission coefficients.

In Fig. 4, it is observed that the radiation efficiency decreases with increasing frequency when $\epsilon = 1.5\epsilon_o$ and $\epsilon = 3\epsilon_o$. The radiation efficiency also decreases when the dielectric constant is increased because a high dielectric material tends to confine more power inside the coaxial when it is exposed to the air on the slot. It is also observed that the radiation efficiency vanishes around the cutoff frequency of the TM_1 mode for the cases with $\epsilon = 6\epsilon_o$ and $\epsilon = 12\epsilon_o$. The radiation efficiency becomes large at the frequencies just above the TM_1 mode cutoff frequency. The operating frequency can be chosen such that both the TEM and the TM_1 modes can propagate to enhance the radiation efficiency at the price of mode dispersion.

In Figs. 5 and 6, we show the effects of slot width on the reflection coefficient and the radiation efficiency. It is observed

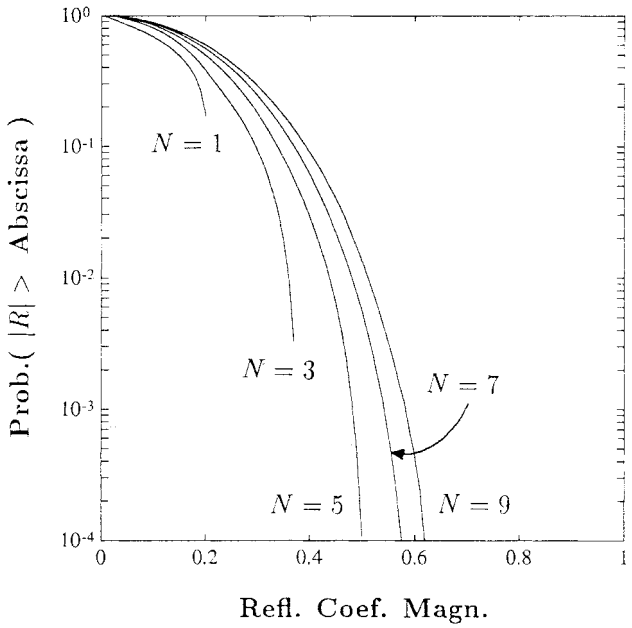

Fig. 11. Probability distribution of the total reflection coefficient caused by $N+1$slots, $f = 8$ GHz, $a = 1.2$ cm, $b = 0.4$ cm, $h_1 = 0.1$ cm, $\epsilon = 1.5\epsilon_o$.

that by increasing the slot width, both the reflection coefficient and the radiation efficiency increase. For the case with $\epsilon = 6\epsilon_o$, the nulls are hardly affected by the slot width.

Figs. 7 and 8 show the effects of the coaxial cable radius with the ratio of outer to inner radii the same. It is observed that the coaxial cable with a smaller radius incurs larger reflection coefficient and radiation efficiency. Since the cutoff frequency of the TM_1 mode with a larger cable radius is lower than that with a smaller radius, nulls are observed for the cases with $a = 2.4$ cm.

In Figs. 9 and 10, we check the effects of radius ratio. As the inner conductor becomes closer to the outer conductor, both the reflection coefficient and the radiation efficiency increase. Also notice that the radiation efficiency has a maximum over the frequency range considered when $b = 0.8$ cm and $b = 1$ cm. For the latter case, the frequency with maximum radiation efficiency is near the high frequency end considered. Although the radiation efficiency is high for the $b = 1$ cm case, its associated reflection coefficient is too high too be of practical use.

Finally, consider the accumulating effect of $N+1$ slots on a coaxial cable. As mentioned in the last section, precise slot locations are impractical to attain to in the gigahertz range, and the phase difference between any two neighboring slots can be approximated to have a uniform distribution over $[0, 2\pi]$. The probability distribution of the reflection coefficient magnitude with 2, 4, 6, 8, and 10 slots are shown in Fig. 11. It is observed that at the same probability level, the total reflection coefficient is smaller than the worst case scenario that all reflection coefficient magnitudes add up. The more slots used, the less increment to the reflection coefficient magnitude is incurred.

VII. Conclusions

We have developed both the Galerkin's and the mode-matching methods to study the reflection and radiation characteristics of a coaxial cable with a circumferential slot. The effects of the dielectric constant and the geometrical parameters are analyzed. It is observed that a total transmission (nulls of both the reflection coefficient and the radiation efficiency) exists around the cutoff frequency of the TM_1 mode. When multiple slots are opened on the cable at random intervals, the accumulated effects on the total reflection coefficient are studied by applying a Monte Carlo simulation, with the results presented as a probability distribution.

Acknowledgment

The author would like to thank Dr. W.-J. Chiu and M.-P. Shih from the Telecommunication Laboratories of Taiwan for their suggestions. The reviewers are deeply appreciated for their useful comments in revising this paper.

References

[1] S. Papatheodorou, J. R. Mautz, and R. F. Harrington, "The aperture admittance of a circumferential slot in a circular cylinder," *IEEE Trans. Antennas Propagat.*, vol. 40, pp. 240–244, Feb. 1992.
[2] T. S. Bird, "Admittance of rectangular waveguide radiating from a conducting cylinder," *IEEE Trans. Antennas Propagat.*, vol. 36, pp. 1217–1220, Sept. 1988.
[3] M.-Y. Li, K. A. Hummer, and K. Chang, "Theoretical and experimental study of the input impedance of the cylindrical cavity-backed rectangular slot antennas," *IEEE Trans. Antennas Propagat.*, vol. 39, pp. 1158–1166, Aug. 1991.
[4] S.-W. Lue, Y. Zhuang, and S.-M. Cao, "The equivalent parameters for the radiating slot on a sectoral waveguide," *IEEE Trans. Antennas Propagat.*, vol. 42, pp. 1577–1581, Nov. 1994.
[5] T. D. Nhat and R. H. MacPhie, "The static electric field distribution between two semi-infinite circular cylinders: a model for the feed gap field of a dipole antenna," *IEEE Trans. Antennas Propagat.*, vol. AP-35, pp. 1273–1280, Nov. 1987.
[6] R. D. Nevels, "The annular aperture antenna with a hemispherical center conductor extension," *IEEE Trans. Antennas Propagat.*, vol. AP-35, pp. 41–45, Jan. 1987.
[7] Y. Wang and D. Fan, "Accurate global solutions of EM boundary-value problems for coaxial radiators," *IEEE Trans. Antennas Propagat.*, vol. 42, pp. 767–770, May 1994.
[8] T. J. Judasz, W. L. Ecklund, and B. B. Balsley, "The coaxial collinear antenna: current distribution from the cylindrical antenna equation" *IEEE Trans. Antennas Propagat.*, vol. AP-35, pp. 327–331, Mar. 1987.
[9] R. F. Harrington, *Time-Harmonic Electromagnetic Fields*. New York: McGraw-Hill, 1993.
[10] J. A. Kong, *Electromagnetic Wave Theory*, 2nd ed. New York: Wiley, 1990.

Jean-Fu Kiang (M'89) was born in Taipei, Taiwan, R.O.C., on February 2, 1957. He received the B.S.E.E. and M.S.E.E. degrees from National Taiwan University and the Ph.D. degree from the Massachusetts Institute of Technology, Cambridge, in 1979, 1981, and 1989, respectively.

He has been with IBM T. J. Watson Research Center, Yorktown Heights, NY, Bellcore, and Siemens. He is now with the Department of Electrical Engineering, National Chung-Hsing University, Taichung, Taiwan.